ACS APPLIED MATERIALS & INTERFACES

Research Article

www.acsami.org

Multilayer Epitaxial Growth of Lead Phthalocyanine and C_{70} Using CuBr as a Templating Layer for Enhancing the Efficiency of Organic Photovoltaic Cells

Tae-Min Kim,[†] Hyun-Sub Shim,[†] Min-Soo Choi,[†] Hyo Jung Kim,[‡] and Jang-Joo Kim*,[†]

[†]Department of Materials Science and Engineering and the Center for Organic Light Emitting Diode, Seoul National University, Seoul 151-744, South Korea

[‡]Department of Organic Material Science and Engineering, College of Engineering, Pusan National University, Busan 609-735, South Korea

Supporting Information

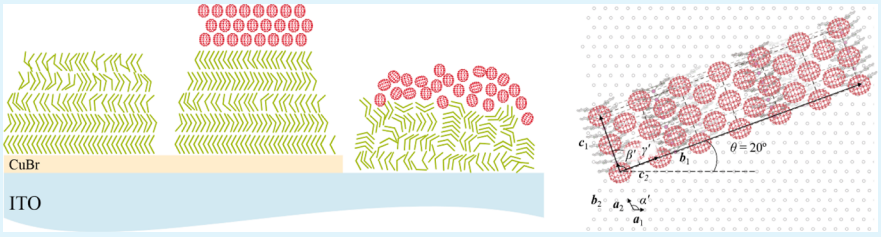

ABSTRACT: The molecular orientation and crystallinity of donor and acceptor molecules are important for high-efficiency organic photovoltaic cells (OPVs) because they significantly influence both the absorption of light and charge-transport characteristics. We report that the templating effect extends to multilayers to increase the crystallinity and to modify the orientation of the crystals of lead phthalocyanine (PbPc) and C_{70} layers at the same time by adopting CuBr as a new templating layer on indium tin oxide (ITO). The formation of a monoclinic phase with a preferred orientation of (320) for PbPc and a fcc phase with a preferred orientation of (220) for C_{70} on the PbPc layer is revealed by X-ray diffraction (XRD) patterns. The multilayer epitaxy results in an increase of the exciton diffusion lengths from 5.6 to 8.8 nm for PbPc and from 6.9 to 13.8 nm for C_{70} to enhance the power conversion efficiency (PCE) of the planar heterojunction OPVs composed of PbPc and C_{70} from 1.4 to 2.3%. The quasi-epitaxy model is proposed to explain the multilayer epitaxy.

KEYWORDS: *organic photovoltaic, templating layer, organic epitaxy, copper bromide, lead phthalocyanine, C_{70}*

1. INTRODUCTION

Tremendous progress has been made in small-molecule-based organic photovoltaic cells (OPVs) in recent years, demonstrating a power conversion efficiency (PCE) up to ~8.9% using the solution process[1−4] and ~8.1% using the vacuum process.[5−8] For the next leap, many researchers are paying attention to the control of the crystal structure and orientation of the molecules because the optical and electrical characteristics of organic films are strongly connected with the crystal structure. The use of templating layers has been considered to be an effective way to control the crystal structure and molecular orientation using intramolecular interactions.[9−12] The molecule−substrate bonding resulting from the electrostatic interactions between molecules and anions in ionic compounds is known to be the driving force to control the crystal structure and to form the preferred orientation of organic molecules.[13−16] Recently, CuI has been successfully used as a templating material to achieve significant enhancement of PCE with classical donor materials.[17−24] However, until now, templating effects have been confined on donor materials deposited on the templating layer. A way to control the phase of the acceptor materials deposited on the donor materials is needed for higher efficiency OPVs.

Here, we demonstrate a multilayer epitaxy by employing CuBr as a templating layer and lead phthalocyanine (PbPc) and C_{70} as the donor and acceptor molecules, respectively. PbPc formed the monoclinic phase with a (320) preferred orientation on CuBr, and the Q-band absorption located in the near-IR region of the molecules is developed by the templating effects.[21] In addition, C_{70} formed the face-centered cubic (fcc) phase with the preferred orientation of (220) when deposited on the crystalline PbPc grown on the CuBr templating layer. The multilayer epitaxy results in the increase of the exciton diffusion lengths (L_D) and the absorption in both layers to enhance the PCE of the planar heterojunction OPVs composed of PbPc and C_{70} from 1.4 to 2.3%.

Received: December 30, 2013
Accepted: February 27, 2014
Published: February 27, 2014

 © 2014 American Chemical Society

2. EXPERIMENTAL SECTION

The organic solar cells used in this study have the following structure: ITO/PbPc (20 nm)/C_{70} (50 nm)/bathocuproine (BCP) (8 nm)/Al (100 nm) with and without a 3 nm thick CuBr layer between the ITO and PbPc layers to investigate the templating effect. The ITO-coated glass substrate was successively cleaned with acetone and isopropyl alcohol, and the substrate was exposed to UV−O_3 for 10 min before use. All of the organic layers were deposited using thermal evaporation at a base pressure of ca. 10^{-7} Torr with a rate of 1 Å/s. The CuBr layer was also deposited using thermal evaporation onto the substrate at a rate of 0.2 Å/s. The aluminum metal cathode was deposited with a rate of 4 Å/s. All of the layers were successively evaporated without breaking the vacuum. The devices had active areas of 2 × 2 mm^2. A patterned insulator on the ITO and the top cathode deposited through a shadow mask defined the cell area. After fabrication, the devices were encapsulated using epoxy resin with glass cans under an N_2 environment. The photovoltaic properties of the devices were measured with an AM 1.5G 100 mW cm^{-2} solar-simulator (300 W Oriel 69911A) light source and a source measurement unit (Keithley 237). The measurement setup was calibrated with a National Renewable Energy Laboratory-certified reference Si solar cell covered with a KG-5 filter before every measurement. More than eight cells for each device structure were fabricated, and the mean values of the photovoltaic performances and standard deviations were obtained. The UV−vis absorption spectra of films were recorded with a VARIAN Cary 5000 UV−vis spectrophotometer. The films were thermally evaporated on UV−O_3-treated ITO substrates. The crystalline structures were investigated by synchrotron X-ray diffraction measurements at the 5A X-ray scattering beamline for materials science at Pohang Light Source II (PLS-II). The X-ray wavelength was 1.071 Å (11.58 KeV) at an incident angle of 0.1°.

3. RESULTS AND DISCUSSION

Figure 1 shows the current density−voltage (J−V) characteristics of the devices measured under light and dark conditions

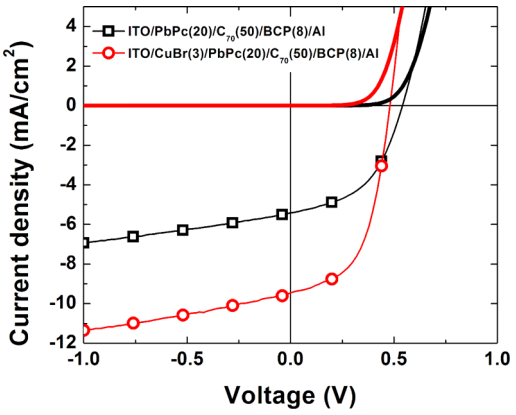

Figure 1. J−V characteristics the OPVs with and without the CuBr layer. The control device (black square) is composed of ITO/PbPc (20 nm)/C_{70} (50 nm)/BCP (8 nm)/Al. The device with a 3 nm thick CuBr (red circle) layer inserted between the ITO and PbPc layers in the control device is shown.

using the illumination of an AM 1.5G 100 mW cm^{-2} solar-simulated light source. The photovoltaic parameters of the devices are summarized in Table 1. J_{SC} was mainly increased by the insertion of CuBr from 5.53 to 9.44 mA cm^{-2}, and the fill factor (FF) was also increased from 0.49 to 0.52. As a result, PCE showed a considerable enhancement of over 1.6 times from 1.45 to 2.34% with the insertion of the CuBr layer despite the slightly reduced open-circuit voltage (V_{OC}) (from 0.53 to 0.48). The origin of the reduction of V_{OC} is not clear yet, but it can be discussed on the basis of the variation of the diode parameters in the devices. V_{OC} in the Shockley diode equation can be expressed as follows[25]

$$V_{OC} = \frac{nkT}{q} \ln\left(\frac{J_{SC}}{J_S}\right) \quad (1)$$

where n is the ideality factor, k is the Boltzmann constant, q is the elementary charge, and J_S is the dark saturation current density. The diode parameters are extracted from the dark J−V characteristic curves and displayed in Table 1. The J_S value increases from 1.57 × 10^{-4} to 3.05 × 10^{-4} mA/cm^2 and n decreases from 2.41 to 1.98 when the CuBr templating layer is used. The calculated V_{OC} values using eq 1 are 0.53 and 0.65 V with and without the CuBr templating layer, respectively, and this tendency is consistent with the change of the measured V_{OC} values of the devices with and without the CuBr layer. Because J_S is a function of the difference between the highest occupied molecular orbital (HOMO) level of the donor and the lowest unoccupied molecular orbital (LUMO) level of the acceptor,[25] the change in the energy-level alignment of the active layers with a CuBr templating layer is a possible origin of the reduction of V_{OC}. Different orientation and different phases have been reported to give different HOMO levels, resulting in different V_{OC} values.[26,27]

To understand the templating effect, the absorption spectra and the incident photon-to-current efficiency (IPCE) spectra of the ITO/PbPc (20 nm) and ITO/CuBr (3 nm)/PbPc (20 nm) films were measured and are shown in Figures 2 and 3, respectively. The absorption peak at a wavelength of 900 nm in the Q-band absorption is more pronounced at the expense of the reduced absorption peak at 740 nm by the insertion of the CuBr layer. This change can be explained by the formation of the monoclinic phase with a (320) preferred orientation, indicating that the CuBr layer acts as a templating layer for the PbPc molecules to enhance the crystallinity of the PbPc film.[21] The IPCE spectrum of the device with the CuBr layer is also broadened in the Q-band region. However, the ratio of the peak intensities at 740 and 900 nm in the IPCE spectrum of the device with CuBr is different from the ratio in the absorption spectrum of the ITO/CuBr (3 nm)/PbPc (20 nm) film. The optical simulation of the devices showed that the difference did not originate from an optical interference effect resulting from stacking additional C_{70}, BCP, and Al layers. The difference can

Table 1. Photovoltaic Parameters of the Solar Cells under AM 1.5G 1 Sun Illumination[a]

	PCE (%)	J_{SC} (mA/cm^2)	V_{OC} (V)	FF	R_P (Ω cm^2)	R_S (Ω cm^2)	n	J_S (mA/cm^2)	calculated V_{OC} (V)
ITO/PbPc(20)/C70(50)/BCP(8)/Al	1.45 ± 0.02	5.53 ± 0.08	0.53 ± 0.02	0.49 ± 0.01	6.47 × 10^6	6.64	2.41	1.57 × 10^{-4}	0.65
ITO/CuBr(3)/PbPc(20)/C70(50)/BCP(8)/Al	2.34 ± 0.10	9.44 ± 0.17	0.48 ± 0.01	0.52 ± 0.03	2.41 × 10^5	9.01	1.98	3.05 × 10^{-4}	0.53

[a]The J_S, R_P, and R_S values were extracted from dark J−V curves using the Schokley diode equation.

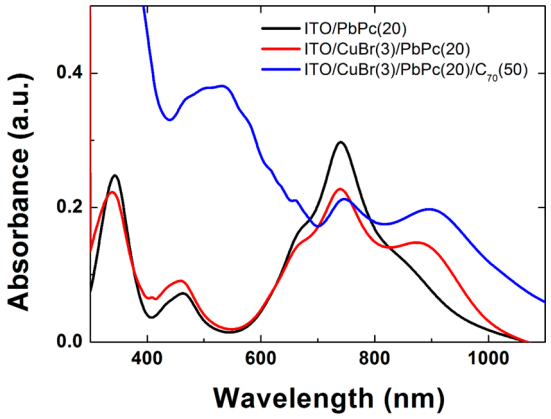

Figure 2. Absorbance spectra of the films with the structures of ITO/PbPc (20 nm), ITO/CuBr (3 nm)/PbPc (20 nm), and ITO/CuBr (3 nm)/PbPc (20 nm)/C_{70} (50 nm) are represented by the black, red, and blue lines, respectively.

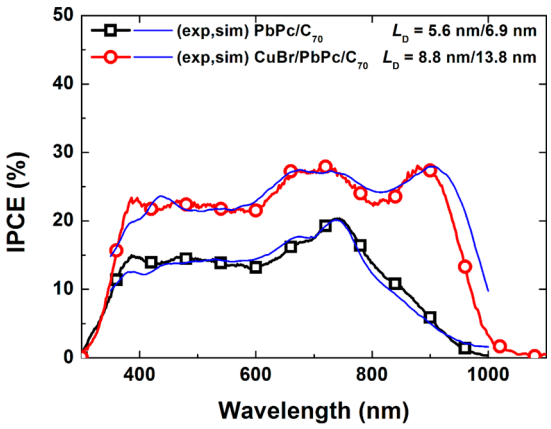

Figure 3. Measured IPCE spectra of the control device (black square) and the device with the CuBr (red circle) templating layer are displayed, and the simulated IPCE spectra using the L_D values shown in the legend are also displayed by the blue lines.

instead be understood from the absorption spectrum of the ITO/CuBr (3 nm)/PbPc (20 nm)/C_{70} (50 nm) film, as shown in Figure 2. Surprisingly, the absorption peak at a wavelength of 900 nm is more broadened and the absorption intensity is also increased after the deposition of C_{70} onto the PbPc layer. In contrast, the absorption peak at a wavelength of 740 nm is reduced again after the deposition of C_{70}. The ratio of the two absorption peak intensities is now in very good agreement with the IPCE spectrum. This result strongly suggests that the PbPc molecules near the surface are rearranged after the deposition of C_{70} onto the PbPc layer. In addition to the modification of the PbPc absorption, the IPCE was also improved in the absorption region of C_{70} by inserting the CuBr layer, implying that the monoclinic phase of the PbPc layer formed by the CuBr interlayer acts as a templating layer for C_{70}. To the best of our knowledge, this is the first time an organic multilayer epitaxy with both donors and acceptors in OPVs using a templating layer has been reported. This effect was not observed in the device based on C_{60}. Even though J_S was increased significantly in the C_{60}-based device by inserting the CuBr layer, the IPCE coming from the C_{60} absorption did not change much (Supporting Information Figure S1). The difference in the lattice constants of the bulk crystal of C_{60} and C_{70} is a possible origin of the different behaviors. The lattice-matching condition between the monoclinic phase of PbPc and the fcc and hexagonal close-packed (HCP) phases of C_{60} was not found from the calculation of dimensionless potential, indicating that quasi-epitaxial growth is not allowed between PbPc and C_{60}.

The formation of the crystals in the PbPc and C_{70} layers resulted in the increase of the L_D values in the layers, increasing the J_{SC} or IPCE. The L_D values in the organic layers were extracted from the fitting of the measured IPCEs using the transfer matrix method with the L_D values as the parameters.[28] For the extraction of L_D, the refractive indices of the 60 and 20 nm thick PbPc films grown on ITO were used for the ITO/CuBr/PbPc and ITO/PbPc films, respectively, because they have similar absorption spectra.[29] The fitting results in Figure 3 showed that the L_D value of the PbPc layer increased from 5.6 ± 0.08 to 8.8 ± 0.13 nm by inserting the CuBr layer, which is consistent with previous results.[18] Moreover, the L_D value of the C_{70} layer was improved by almost a factor of 2, from 6.9 ± 0.10 to 13.8 ± 0.21 nm, also by the insertion of the CuBr layer. As a result, the J_{SC} value of the device increased by 1.7 times, from 5.53 to 9.44 mA cm^{-2}.

The structural change of the molecules was investigated using the X-ray diffraction (XRD) patterns shown in Figure 4a. The diffraction pattern of the 20 nm thick PbPc layer deposited on an ITO substrate showed two peaks near Q = 9 and 11.67 nm^{-1}, which can be assigned as the mixture of the (320)-oriented monoclinic phase (Q = 8.81 nm^{-1}), the $(1\bar{2}1)$-oriented triclinic phase (Q = 9.12 nm^{-1}), and the $(1\bar{3}0)$-oriented triclinic phase (Q = 11.67 nm^{-1}).[21,29] When the PbPc was grown on the ITO/CuBr (3 nm), the crystallinity of the monoclinic phase and the $(1\bar{2}1)$-oriented triclinic phase was increased and the amount of the $(1\bar{3}0)$-oriented triclinic phase was reduced. However, the 50 nm thick C_{70} layer deposited on ITO has a fcc structure with a (111) preferred orientation identified by the diffraction peak at Q = 7.36 nm^{-1}. Interestingly, the intensity of the C_{70} peaks was intensified and the PbPc peaks disappeared when the C_{70} layer was grown on the ITO/PbPc layer. This fact indicates that the crystallinity of the underlying PbPc layer was demolished by the deposition of the C_{70} on top of PbPc, clearly demonstrating that the overlayer of C_{70} significantly modified the structure of the underlying layer. In contrast, the crystallinity of the PbPc layer grown on the ITO/CuBr remained with slight modification of the structure after the deposition of the C_{70} layer. Furthermore, the diffraction peak near Q = 9 nm^{-1} of the PbPc layer becomes stronger after the deposition of the C_{70} layer onto the PbPc film, strongly suggesting that the crystallinity of the PbPc layer was increased by the deposition of the C_{70} layer, which was manifested from the comparison of the intensities of the peaks near Q = 9 nm^{-1} in Figure 4b. In addition, the (220)-oriented fcc C_{70} phase increased at the expense of the reduced amount of the (111)-oriented fcc phase in the C_{70} layer. These results are consistent with the increase of the absorption intensity at a wavelength of 940 nm via the deposition of C_{70}. This kind of reconstruction of the organic molecules during Stranski–Krastanov growth in a heteroepitaxy system was also reported by Barrena et al.[30] The crystalline structure can be modified by the strain energy induced from the lattice mismatch between the substrate and overlayer in an organic heteroepitaxy system because organic films are softer than inorganic flms. These results can be summarized as follows: (1) CuBr acts as a templating layer to increase the crystallinity of the PbPc layer, (2) the crystalline PbPc layer acts as a templating layer for C_{70}

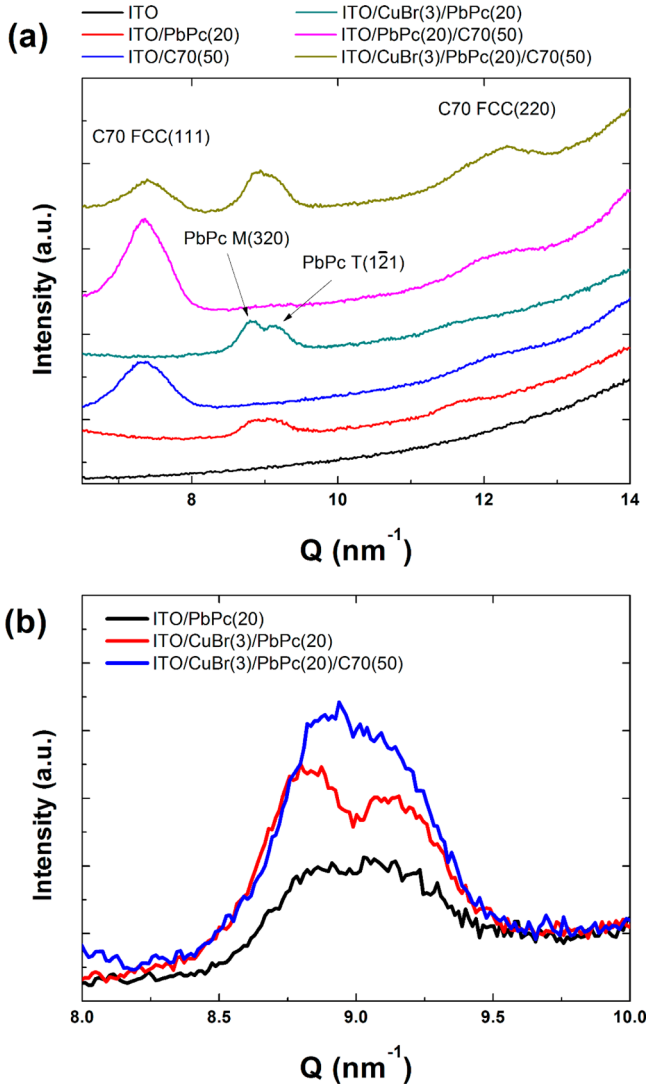

Figure 4. (a) XRD profiles of the films with the following structures: ITO/PbPc (20 nm), ITO/CuBr (3 nm)/PbPc (20 nm), ITO/C_{70} (50 nm), ITO/PbPc (20 nm)/C_{70} (50 nm), and ITO/CuBr (3 nm)/PbPc (20 nm)/C_{70} (50 nm). The peaks of monoclinic PbPc with a (320) orientation and fcc C_{70} with (111) and (220) orientations are also displayed. (b) Comparison of the peaks of the ITO/PbPc (20 nm), ITO/CuBr (3 nm)/PbPc (20 nm), and ITO/CuBr (3 nm)/PbPc (20 nm)/C_{70} (50 nm)films near Q = 9 nm^{-1}.

molecules to form crystals with a preferred (220) orientation, and (3) the crystallinity of the PbPc bottom layer is increased by the deposition of the C_{70} overlayer. The growth mode is schematically represented by the cartoon images in Figure 5.

The templating effect can be explained by the model of quasi-epitaxial growth in organic films, where the dimensionless potential, V/V_0, representing the lattice matching between the substrate and the overlayer, is used as the parameter.[15] The value of V/V_0 is determined by the degree of commensurism between the overlayer and the substrate in the range $-0.5 \leq V/V_0 \leq 1$. $V/V_0 = 1$ for incommensurism, $V/V_0 = 0.5$ for coincidence, and $V/V_0 = 0$ and $V/V_0 = -0.5$ for commensurism on nonhexagonal and hexagonal substrates, respectively. The lattice parameters of zinc blende CuBr, monoclinic PbPc, and fcc C_{70} are summarized in Table 2.[31−33] The potential V/V_0 values between the (111) plane of the CuBr crystal and the (320) plane of the monoclinic PbPc crystal and between the

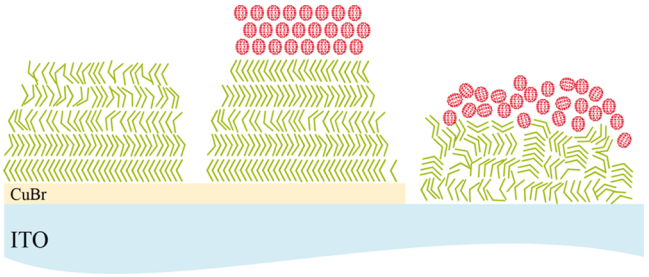

Figure 5. Cartoon image of multilayer epitaxy film composed of ITO/CuBr/PbPc, ITO/CuBr/PbPc/C_{70}, and ITO/PbPc/C_{70}.

Table 2. Lattice Parameters of Zinc Blende CuBr, Monoclinic PbPc, and fcc C_{70}

	a (Å)	b (Å)	c (Å)	$\alpha = \beta = \gamma$ (deg)
CuBr	5.695	5.695	5.695	90
PbPc monoclinic	25.48	25.48	3.73	90
C_{70} fcc	14.89	14.89	14.89	90

(320) plane of the monoclinic PbPc crystal and the (220) plane of the fcc C_{70} crystal were calculated against the azimuthal angle (θ) and displayed in Figure 6a. The angle θ was defined as the angle between vectors a_1 and b_1, with b_1 and c_1 defining the

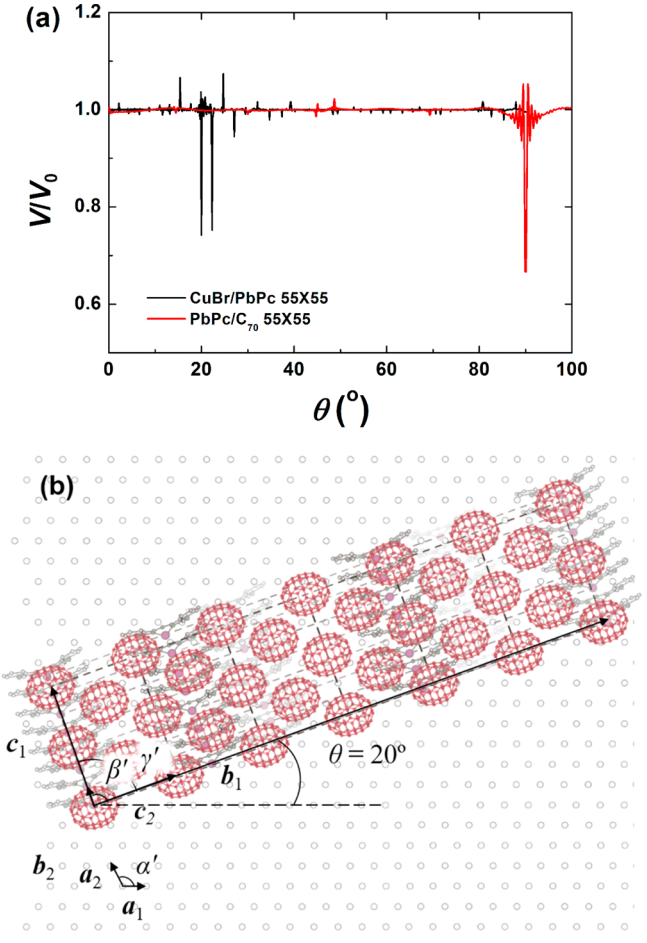

Figure 6. (a) Calculated dimensionless potential, V/V_0, of CuBr (111)/PbPc monoclinic (320) and PbPc monoclinic (320)/C_{70} FCC (220). (b) Schematic representation of PbPc monoclinic (320) and C_{70} fcc (110) unit cells on zinc blende CuBr (111).

dx.doi.org/10.1021/am405946m | ACS Appl. Mater. Interfaces 2014, 6, 4286−4291

azimuthal angles between the overlayer and substrate in Figure 6b. The size of the overlayer was 55 × 55. The results clearly show that the minimum potential between the (111) plane of the CuBr crystal and the (320) plane of the monoclinic PbPc crystal are derived at an angle of 20°. The minimum potential between the (320) plane of the monoclinic PbPc crystal and the (220) plane of the C_{70} crystal was obtained at an angle of 90°. The arrangement of CuBr, PbPc. and C_{70} are schematically represented in Figure 6b, exhibiting the multilayer epitaxy.

4. CONCLUSIONS

We demonstrated multilayer epitaxy composed of ITO/CuBr/PbPc/C_{70} and successfully fabricated OPVs with multilayer epitaxy films. The CuBr layer worked well as a templating layer to form the monoclinic PbPc molecules. In addition, the crystallized PbPc molecules act as a templating layer for the C_{70} overlayer. As a result, the L_D values of the PbPc and C_{70} layers were improved at the same time, from 5.6 to 8.8 nm for PbPc and from 6.9 to 13.8 nm for C_{70}. As a result, the OPV device with CuBr showed a 1.6-fold enhancement in the PCE, which resulted from the increase in the J_{SC} value. Furthermore, the results from the calculations of the dimensionless potential, V/V_0, for the layers show that the templating effects of each layer can be explained by quasi-epitaxial growth.

The increment of the exciton diffusion length in both donor and acceptor layers has been a major issue in increasing the short-circuit current in organic solar cells. The multilayer epitaxy demonstrated in this study not only explains the origin of the effect of the templating layer on the organic (donor) layer to control its crystal structure but also extends the concept of epitaxy to the organic/organic multilayers to improve the light harvesting from the overlying organic (acceptor) layer. This multilayer epitaxy method can easily be extended to other sets of materials with known lattice parameters of organic crystals and will generally contribute to finding a proper combination of materials, for instance, to develop new templating materials and acceptor molecules for a given excellent donor material or vice versa to improve the performance of OPVs.

■ ASSOCIATED CONTENT

Supporting Information

J–*V* characteristic curves and IPCE spectra of the organic solar cells with C_{60} measured with an AM 1.5G 100 mW cm^{-2} solar-simulator light source. This material is available free of charge via the Internet at http://pubs.acs.org.

■ AUTHOR INFORMATION

Corresponding Author

*E-mail: jjkim@snu.ac.kr.

Notes

The authors declare no competing financial interest.

■ ACKNOWLEDGMENTS

This work was supported by a New & Renewable Energy Technology Development Program of the Korea Institute of Energy Technology Evaluation and Planning (KETEP) grant funded by the Korean government's Ministry of Knowledge Economy (no. 20113020010070).

■ REFERENCES

(1) Sun, Y.; Welch, G. C.; Leong, W. L.; Takacs, C. J.; Bazan, G. C.; Heeger, A. J. Solution-Processed Small-Molecule Solar Cells with 6.7% Efficiency. *Nat. Mater.* **2012**, *11*, 44–48.

(2) Li, Z.; He, G.; Wan, X.; Liu, Y.; Zhou, J.; Long, G.; Zuo, Y.; Zhang, M.; Chen, Y. Solution Processable Rhodanine-Based Small Molecule Organic Photovoltaic Cells with a Power Conversion Efficiency of 6.1%. *Adv. Energy Mater.* **2012**, *2*, 74–77.

(3) Huang, J.; Zhan, C.; Zhang, X.; Zhao, Y.; Lu, Z.; Jia, H.; Jiang, B.; Ye, J.; Zhang, S.; Tang, A.; Liu, Y.; Pei, Q.; Yao, J. Solution-Processed DPP-Based Small Molecule that Gives High Photovoltaic Efficiency with Judicious Device Optimization. *ACS Appl. Mater. Interfaces* **2013**, *5*, 2033–2036.

(4) Kyaw, A. K. K.; Wang, D. H.; Wynands, D.; Zhang, J.; Nguyen, T.-Q.; Bazan, G. C.; Heeger, A. J. Improved Light Harvesting and Improved Efficiency by Insertion of an Optical Spacer (ZnO) in Solution-Processed Small-Molecule Solar Cells. *Nano Lett.* **2013**, *13*, 3796–3801.

(5) Chiu, S.-W.; Lin, L.-Y.; Lin, H.-W.; Chen, Y.-H.; Huang, Z.-Y.; Lin, Y.-T.; Lin, F.; Liu, Y.-H.; Wong, K.-T. A Donor–Acceptor–Acceptor Molecule for Vacuum-Processed Organic Solar Cells with a Power Conversion Efficiency of 6.4%. *Chem. Commun.* **2012**, *48*, 1857–1859.

(6) Chen, G.; Sasabe, H.; Wang, Z.; Wang, X.-F.; Hong, Z.; Yang, Y.; Kido, J. Co-Evaporated Bulk Heterojunction Solar Cells with > 6.0% Efficiency. *Adv. Mater.* **2012**, *24*, 2768–2773.

(7) Fitzner, R.; Mena-Osteritz, E.; Mishra, A.; Schulz, G.; Reinold, E.; Weil, M.; Körner, C.; Ziehlke, H.; Elschner, C.; Leo, K.; Riede, M.; Pfeiffer, M.; Uhrich, C.; Bäuerle, P. Correlation of π-Conjugated Oligomer Structure with Film Morphology and Organic Solar Cell Performance. *J. Am. Chem. Soc.* **2012**, *134*, 11064–11067.

(8) Xiao, X.; Bergemann, K. J.; Zimmerman, J. D.; Lee, K.; Forrest, S. R. Small-Molecule Planar-Mixed Heterojunction Photovoltaic Cells with Fullerene-Based Electron Filtering Buffers. *Adv. Energy Mater.* [Online early access]. DOI: 10.1002/aenm.201301557. Published Online: Dec 23, 2013.

(9) Yu, B.; Huang, L.; Wang, H.; Yan, D. Efficient Organic Solar Cells Using a High-Quality Crystalline Thin Film as a Donor Layer. *Adv. Mater.* **2010**, *22*, 1017–1020.

(10) Sakurai, T.; Ohashi, T.; Kitazume, H.; Kubota, M.; Suemasu, T.; Akimoto, K. Structural Control of Organic Solar Cells Based on Nonplanar Metallophthalocyanine/C60 Heterojunctions Using Organic Buffer Layers. *Org. Electron.* **2011**, *12*, 966–973.

(11) Zhao, W.; Mudrick, J. P.; Zheng, Y.; Hammond, W. T.; Yang, Y.; Xue, J. Enhancing Photovoltaic Response of Organic Solar Cells Using a Crystalline Molecular Template. *Org. Electron.* **2012**, *13*, 129–135.

(12) Roy, S. S.; Bindl, D. J.; Arnold, M. S. Templating Highly Crystalline Organic Semiconductors Using Atomic Membranes of Graphene at the Anode/Organic Interface. *J. Phys. Chem. Lett.* **2012**, *3*, 873–878.

(13) Koma, A. Molecular Beam Epitacxial Growth of Organic Thin Films. *Prog. Cryst. Growth Charact.* **1995**, *30*, 129–152.

(14) Forrest, S. R. Ultrathin Organic Films Grown by Organic Molecular Beam Deposition and Related Techniques. *Chem. Rev.* **1997**, *97*, 1793–1896.

(15) Hooks, D. E.; Fritz, T.; Ward, M. D. Epitaxy and Molecular Organization on Solid Substrates. *Adv. Mater.* **2001**, *13*, 227–241.

(16) Yang, J.; Yan, D. Weak Epitaxy Growth of Organic Semiconductor Thin Films. *Chem. Soc. Rev.* **2009**, *38*, 2634–2645.

(17) Cheng, C. H.; Wang, J.; Du, G. T.; Shi, S. H.; Du, Z. J.; Fan, Z. Q.; Bian, J. M.; Wang, M. S. Organic Solar Cells with Remarkable Enhanced Efficiency by Using a CuI Buffer To Control the Molecular Orientation and Modify the Anode. *Appl. Phys. Lett.* **2010**, *97*, 083305-1–083305-3.

(18) Shim, H.-S.; Kim, H. J.; Kim, J. W.; Kim, S.-Y.; Jeong, W.-I.; Kim, T.-M.; Kim, J.-J. Enhancement of Near-Infrared Absorption with High Fill Factor in Lead Phthalocyanine-Based Organic Solar Cells. *J. Mater. Chem.* **2012**, *22*, 9077–9081.

(19) Kim, T.-M.; Kim, J. W.; Shim, H.-S.; Kim, J.-J. High Efficiency and High Photo-Stability Zinc-Phthalocyanine Based Planar Heterojunction Solar Cells with a Double Interfacial Layer. *Appl. Phys. Lett.* **2012**, *101*, 113301-1−113301-5.
(20) Rand, B. P.; Cheyns, D.; Vasseur, K.; Giebink, N. C.; Mothy, S.; Yi, Y.; Coropceanu, V.; Beljonne, D.; Cornil, J.; Brédas, J.-L.; Genoe, J. The Impact of Molecular Orientation on the Photovoltaic Properties of a Phthalocyanine/Fullerene Heterojunction. *Adv. Funct. Mater.* **2012**, *22*, 2987−2995.
(21) Kim, H. J.; Shim, H.-S.; Kim, J. W.; Lee, H. H.; Kim, J.-J. CuI Interlayers in Lead Phthalocyanine Thin Films Enhance Near-Infrared Light Absorption. *Appl. Phys. Lett.* **2012**, *100*, 263303-1−263303-4.
(22) Zhou, Y.; Taima, T.; Miyadera, T.; Yamanari, T.; Kitamura, M.; Nakatsu, K.; Yoshida, Y. Glancing Angle Deposition of Copper Iodide Nanocrystals for Efficient Organic Photovoltaics. *Nano Lett.* **2012**, *12*, 4146−4152.
(23) Kim, J. W.; Kim, H. J.; Kim, T.-M.; Kim, T. G.; Lee, J.-H.; Kim, J. W.; Kim, J.-J. High Performance Organic Planar Heterojunction Solar Cells by Controlling the Molecular Orientation. *Curr. Appl. Phys.* **2013**, *13*, 7−11.
(24) Vasseur, K.; Broch, K.; Ayzner, A. L.; Rand, B. P.; Cheyns, D.; Frank, C.; Schreiber, F.; Toney, M. F.; Froyen, L.; Heremans, P. Controlling the Texture and Crystallinity of Evaporated Lead Phthalocyanine Thin Films for Near-Infrared Sensitive Solar Cells. *ACS Appl. Mater. Interfaces* **2013**, *5*, 8505−8515.
(25) Potscavage, W. J., Jr.; Sharma, A.; Kippelen, B. Critical Interfaces in Organic Solar Cells and Their Influence on the Open-Circuit Voltage. *Acc. Chem. Res.* **2009**, *42*, 1758−1767.
(26) Chen, W.; Qi, D.-C.; Huang, H.; Gao, X.; Wee, T. S. Organic−Organic Heterojunction Interfaces: Effect of Molecular Orientation. *Adv. Funct. Mater.* **2011**, *21*, 410−424.
(27) Placencia, D.; Wang, W.; Shallcross, R. C.; Nebesny, K. W.; Brumbach, M.; Armstrong, N. R. Organic Photovoltaic Cells Based on Solvent-Annealed, Textured Titanyl Phthalocyanine/C60 Heterojunctions. *Adv. Funct. Mater.* **2009**, *19*, 1913−1921.
(28) Lee, J.; Kim, S.-Y.; Kim, C.; Kim, J.-J. Enhancement of the Short Circuit Current in Organic Photovoltaic Devices with Microcavity Structures. *Appl. Phys. Lett.* **2010**, *97*, 083306-1−083306-3.
(29) Vasseur, K.; Rand, B. P.; Cheyns, D.; Froyen, L.; Heremans, P. Structural Evolution of Evaporated Lead Phthalocyanine Thin Films for Near-Infrared Sensitive Solar Cells. *Chem. Mater.* **2011**, *23*, 886−895.
(30) Barrena, E.; de Oteyza, D. G.; Sellner, S.; Helmut, D. In Situ Study of the Growth of Nanodots in Organic Heteroepitaxy. *Phys. Rev. Lett.* **2006**, *97*, 076102-1−076102-4.
(31) Ukei, K. Lead Phthalocyanine. *Acta Crystallogr., Sect. B: Struct. Crystallogr. Cryst. Chem.* **1973**, *29*, 2290−2292.
(32) Hull, S.; Keen, D. A. High-Pressure Polymorphism of the Copper(I) Halides: A Neutron-Diffraction Study to ∼10 GPa. *Phys. Rev. B* **1994**, *50*, 5868−5885.
(33) Valsakumar, M. C.; Subramanian, N.; Yousuf, M.; Sahu, P. Ch.; Hariharan, Y.; Bharathi, A.; Sankara Sastry, V.; Janaki, J.; Rao, G. V. N.; Radhakrishnan, T. S.; Sundar, C. S. Crystal Structure and Disorder in Solid C70. *Phys. Rev. B* **1993**, *48*, 9080−9085.